Effects of two-stage harvesting soil loosening mechanism rotary tillage blade on *Fritillaria ussuriensis* Maxim collision damage

Jiang Song[1], Yaoshen Wang[1], Yiyong Han[2*], Bo Ma[3], Jingyang Bian[4], Sibo Wang[1], Shuai Tian[1]

(1. *College of Engineering, Heilongjiang Bayi Agricultural University, Daqing 163319, China*;
2. *College of Traffic and Transportation, Nanning University, Nanning 530200, China*;
3. *Qiqihaer Branch of Heilongjiang Academy of Agricultural Sciences, Qiqihaer 161006, China*;
4. *Daqing Branch of Heilongjiang Academy of Agricultural Sciences, Daqing 163319, China*)

Abstract: A two-stage harvester is one method for achieving high-efficiency and low-loss mechanized harvesting of *Fritillaria ussuriensis* Maxim (FUM), a perennial herb. To address the poor performance of the soil breaking mechanism, the soil breaking performance can be improved by adding a rotary tillage blade set based on the existing soil breaking mechanism; however, it easily causes damage to the FUM. Therefore, in this study, a numerical simulation method was used to obtain the minimum FUM energy loss and minimum damage when the width of the rotary tillage blade cutter edge was 8 mm. A FUM rotary-tillage blade collision damage test bed was built, and the influence of the rotational speed, cutter edge width, and collision direction on the FUM mass loss ratio was analyzed using a random block test. The results of the random block test showed that the influencing factor model of the FUM mass loss ratio was significant. The rotational speed and width had a significant influence on the mass loss ratio, and the collision direction only had a significant influence on the free FUM. The results of the single-factor test showed that the mass loss ratio was proportional to the rotational speed, and that it increased as the rotational speed increased. The order of influence of the collision direction on the mass loss ratio was *Y*>*X*>*Z*. The variation in the mass loss ratio and cutter edge width indicated that the mass loss ratio of the 8 mm-wide cutter edge was the smallest. The minimum damage caused by the 8 mm-wide cutter edge was also determined. The results of this study can provide a theoretical reference for the appropriate rotational speed of the low-loss soil-loosening mechanism in FUM topsoil stripping machines and the structural design of the rotary tillage blade.

Keywords: *Fritillaria ussuriensis* Maxim, two-stage harvester, soil-loosening mechanism, low-loss
DOI: 10.25165/j.ijabe.20251806.8990

Citation: Song J, Wang Y S, Han Y Y, Ma B, Bian J Y, Wang S B, et al. Effects of two-stage harvesting soil loosening mechanism rotary tillage blade on *Fritillaria ussuriensis* Maxim collision damage. Int J Agric & Biol Eng, 2025; 18(6): 83–93.

1 Introduction

Fritillaria ussuriensis Maxim (FUM) is a perennial herb belonging to the *Fritillaria* genus of the lily family. Its underground bulbs are harvested for their medicinal value[1], and they have an average size of 3-30 mm and a harvest depth of 70-100 mm. FUM is flat in shape, with two outer scales similar in size or slightly different in size, and a small central scale[2]. As an herbal medicine, FUM relieves cough and reduces phlegm[3,4]. According to statistical data, the planting area of FUM is 10 000 hm^2, and the annual economic benefits amount to more than one billion RMB[5].

Currently, FUM harvesting is primarily based on high-intensity labor, which results in low work efficiency and high labor costs. Because of the high labor costs, mechanized harvesting of FUM is urgently needed. Rotary tillage is an operational method with excellent soil-breaking effects. Accordingly, extensive research on the soil breaking quality of rotary tillage has been conducted. Specifically, researchers have improved the quality of crushed soil by improving the structure of rotary tillage blades. For example, Lee et al.[6] studied the tillage characteristics of a rotary tillage blade in a dryland direct seeding machine for rice and found that the scimitar exhibited a favorable soil breaking performance in wetland paddy fields, with the four-blade rotor having the highest breaking rate. In addition, Guo et al.[7] improved the IT225 rotary blade based on bionic theory, and the field test results showed that the soil breakage rate of the improved blade was better than that before the improvement under different operating conditions. Furthermore, Yang et al.[8] designed a bionic rotary tillage blade with a multi-toe structure. The experimental results showed that this structure could effectively reduce the fracture radius of the soil. Moreover, Jia et al.[9] found that reducing the positive cutting edge angle, sliding cutting angle, and blade thickness improved the quality of crushed soil, and that increasing the blade thickness significantly reduced the quality of crushed soil. Zhang et al.[10] simulated a blade-soil-straw interaction model using the discrete element method, and the test results indicated that the transition edge angle α was too small for the blade to effectively cut the soil, and the larger the bending angle β, the higher the cutting performance. Zhao et al.[11] used the discrete element method to study the effects of different edge geometries on torque demand and soil disturbance characteristics, and found that a superior soil cutting performance and lower torque requirements could be achieved by using a larger slip cutting angle.

Received date: 2024-04-09 **Accepted date:** 2025-08-05
Biographies: **Jiang Song**, Professor, research interest: agricultural mechanization, Email: songjiang@byau.edu.cn; **Yaoshen Wang**, MS candidate, research interest: agricultural mechanization, Email: wangyaoshen@byau.edu.cn; **BoMa**, Researcher, research interest: agricultural mechanization, Email: mabo8210@163.com; **Jingyang Bian**, Researcher, research interest: agricultural mechanization, Email: bjy19800926@163.com; **Sibo Wang**, MS candidate, research interest: agricultural mechanization, Email: 13945713646@163.com; **Shuai Tian**, MS candidate, research interest: agricultural mechanization, Email: tianshuai@hljbynkdx17.wecom.work.

***Corresponding author: Yiyong Han**, Professor, research interest: agricultural mechanization. College of Traffic and Transportation, Nanning University, Nanning 530200, China. Tel: +86-13877587766, Email: hanyiyong@unn.edu.cn.

Additionally, researchers have improved the quality of crushed soil by improving the motion parameters of rotary tillage blades. For example, Matin et al.[12-14] studied the tillage method of rotary tillage cutlery, and found that the soil breakage rate increased as the rotational speed of the rotary tillage blade increased. In addition, Jiang et al.[15] conducted a whole-machine test with a seedling bed preparation machine, and the field test results demonstrated that the rotational speed of the rotary tillage device had a significant effect on the soil breakage rate, which increased as the rotational speed increased. Furthermore, Yang et al.[16] conducted simulations and experimental studies on a variety of rotary tillage blades at different rotational speeds to clarify the mechanism through which the blades and the soil interact during strip rotary tillage. They found not only that increases in the rotational speed improved the soil crushing performance, but also that curved rotary tillage blades produced the best soil crushing effect.

Through bionic design, theoretical analysis, and other methods, researchers have studied the effects of the structural and motion parameters of rotary tillage blades on the soil crushing quality. The results described above indicate that curved rotary tillage blades are more effective for breaking the soil, that increasing the rotational speed of the rotary tillage blade can improve the soil breaking effect, and that optimizing the blade angle, side cutting edge, and sliding cutting angle also improves the soil cutting effect.

In summary, based on the existing soil-loosening mechanisms, the addition of a rotary tillage tool group can improve the soil breaking effect. However, the soil-loosening mechanism handles a mixture of the FUM and soil. Rotation speeds that are too fast and rotary tillage blades that are too sharp can cause significant damage to the FUM. Therefore, it is necessary to study the structural and motion parameters of rotary tillage blades to minimize the damage to the FUM and improve the soil crushing effect.

There are few studies that address damage to FUM. Current research is focused on the collision damage caused by the harvesting equipment. For example, Li et al.[17,18] investigated the collision damage inflicted on FUM in the screening process by conducting a drop collision test, which was compared to a finite element analysis. The results revealed the optimal values of the motion parameters, which were used to reduce the collision damage between the screen and FUM. In addition, Song et al.[19,20] used the free fall and pendulum methods to analyze the collision damage to FUM during harvesting. They found that the fall height, collision material, collision direction, and the number of collisions had a significant impact on the extent of the damage, and that the impact of the damage could be reduced by adjusting the internal structure of the roller screen. However, these studies only focused on the collision damage inflicted on FUM during the harvesting process. There are few reports on the structure and parameters of the damage caused to FUM by soil-loosening equipment and rotary tillage blades.

In this study, the relationship between FUM damage and the structure and motion parameters of the rotary tillage blade was investigated in order to clarify the low-loss loose mechanism of FUM. It provides theoretical basis and technical reference for the development of FUM topsoil peeler with low FUM damage and high-quality crushed soil.

2 Materials and methods

2.1 Soil-loosening mechanism of FUM topsoil stripping machine

Currently, the special cash crop innovation team of Heilongjiang Bayi Agricultural University has developed a two-stage FUM harvester[21], which consists of a FUM topsoil stripper and a drum FUM screening machine. The FUM topsoil stripper includes a screw unit, cone gear reducer, scraper, soil relief hook, side plate, transmission system, frame, straight gear reducer, and three-point suspension. The spiral device is located at the front end of the cardigan topsoil stripper and is installed under the frame. The scraper is located near the rear of the screw device and is connected to the frame. A soil relief hook is mounted on the side plate connected to the beam. The frame is connected to a tractor using a three-point suspension. One end of the tapered gear reducer is connected to the straight gear reducer of the spiral device through a chain, and the other end is connected to the drive shaft and tractor power output shaft. During operation, the tractor drives the FUM topsoil stripping machine forward, the soil-splitting screw mechanism peels the soil covering the surface to either side, and the soil-loosening mechanism loosens the FUM soil layer. The structure and operational effects of the entire machine are shown in Figure 1. Because the operation of the soil-loosening mechanism is not completely thorough, large soil particles are left behind. Therefore, the soil-loosening mechanism needs to be improved.

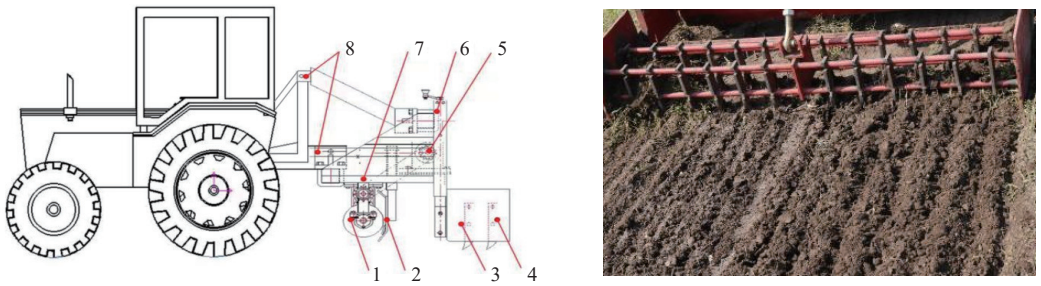

a. FUM topsoil stripping machine b. Soil-loosening operation

1.screw device 2.scraper plate 3.side plate 4.soil-loosening hook 5.taper gear reducer 6.frame of machine 7.straight gear reducer 8.three-point suspension.

Figure 1 FUM topsoil stripping machine and operation

The modified soil-loosening mechanism consists of soil-loosening hook and rotary tillage blade (Figure 2). The entire machine was driven by a tractor with a working width of 1.3 m. The soil-loosening hook group consisted of a row of soil-loosening hooks to initially loosen the soil while the machine moved forward. A spacing between the soil-loosening hooks that is too small causes soil accumulation. Based on the actual situation, the minimum distance between soil accumulations was 10 cm. As the distance increased, the FUM between the soil-loosening hooks was not disturbed, and the FUM was still rooted in the soil; this is called the

"fixed state". The disturbed FUM separated from the soil is considered to be in the "free state". The rotary tillage blade group consisted of multiple cutterheads with rotary tillage blades, and there was a phase angle between the cutter. The rotary tillage blade group was driven by a hydraulic motor to rotate the soil and ensure it was completely loosened. This study focuses on the rotary tillage blade at the rear of the machine and examines the damage caused to the FUM by the rotary tillage blade during operation.

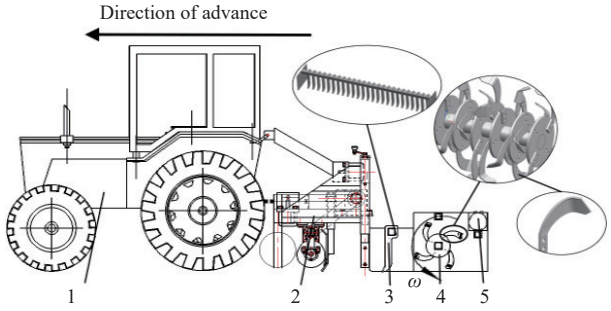

1.tractor 2.topsoil stripping machine 3.soil-loosening hook group 4.rotary tillage blade group 5.hydraulic motor.

Figure 2 FUM topsoil stripping machine

The structure of the rotary tillage blade used in the test and its size is shown in Figure 3.

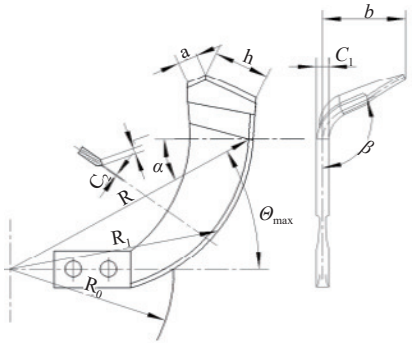

Structure	Dimensions
R	195 mm
R_0	120 mm
R_1	150 mm
C_1	5 mm
C_2	2 mm
a	16 mm
b	62 mm
L	16 mm
h	40 mm
α	30°
β	115°
Θ_{max}	30°

Figure 3 Diagram of rotary tillage blade structure

2.2 Test materials

The FUM and soil used in the experiment were obtained from Tieli City, Heilongjiang Province, China. The FUM was harvested manually, mixed with soil to prevent deterioration during storage, transported to the special crop equipment laboratory of Heilongjiang Bayi Agricultural University, and stored in a freezer. The storage temperature was 2°C-6°C and the humidity was approximately 13%-14%[22]. Before the experiment was initiated, the FUM was cleaned, and visual inspection confirmed that the FUM had no damage.

The test examining the collision between the FUM and the rotary tillage blade was completed in August 2023 at the special crop equipment laboratory of the College of Engineering of Heilongjiang Bayi Agricultural University. This experiment focused on the extent of the FUM damage and the measurable results of the collision between the FUM and the rotary tillage blade. The FUM mass loss ratio was selected as the performance index. Considering that the quality, size, and shape of FUM have a significant influence on its mass loss ratio, FUM bulbs with minimal differences in size and shape were selected as the test materials. For the mass measurements, an electronic scale (CN-LQC3002, Lucky, China) with an accuracy of 0.01 g was used, with a single particle weight of 3.5±0.5 g.

2.3 Test method

2.3.1 FUM collision damage test bench

As shown in Figure 4, a rectangular coordinate system was established for statistical convenience. The FUM was placed on a horizontal surface with the roots facing down. The plane in which the FUM root system was located was considered the reference plane, the gap in which the two petals were clasped was considered the y-axis, and the vertical y-axis in the horizontal plane was considered the x-axis. The vertical x- and y-axes formed the z-axis, and the vertical plane was upward.

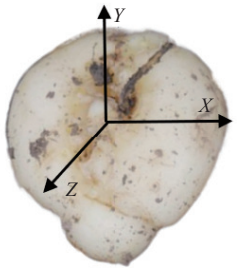

Figure 4 Example of FUM cartesian coordinate system

To reduce the influence of external factors during collisions, FUM rotary tillage blade collision test benches were designed. It is difficult to directly measure the damage inflicted on FUM in the planting field; therefore, the damage to the FUM was determined via a collision test involving the FUM rotary tillage blade. As shown in Figure 5, the test bench was welded to a steel structure that was primarily composed of a support beam, connecting rod, rotary tillage blade, threaded rod, bearing, plastic bench, and test groove. The support beam was welded to the base frame, and the bearing and support were attached using a connecting rod with threads. After the connecting rod completed the dynamic balance adjustment, the end of the rod was connected to the rotary tillage blade. The test groove was placed on a plastic bench, and its position was adjusted to allow the FUM located in the groove to collide with the end of the rotary tillage blade. In the test, the rotary tillage blade was released at different heights (determined using a tape measure), circular motion around the threaded rod was ensured under the guidance of the connecting rod, and the collision with the FUM was executed at the lowest point.

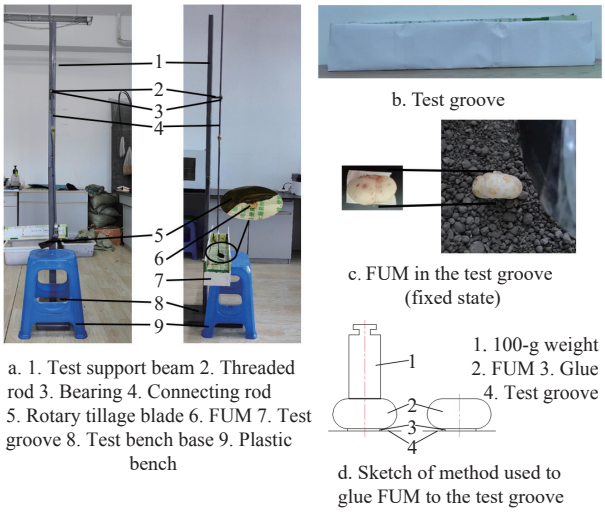

a. 1. Test support beam 2. Threaded rod 3. Bearing 4. Connecting rod 5. Rotary tillage blade 6. FUM 7. Test groove 8. Test bench base 9. Plastic bench

Figure 5 Bench used for collision test of FUM and rotary tillage blade

To simulate the fixed and free states of FUM, the FUM and the test groove were glued together and pressed with a constant force of

a weight of 100 g (only the state of the fixed FUM). This ensured that the FUM was glued to the groove but was still able to escape from the adhesion when disturbed by a sufficiently large force.

The equivalent collision height (h) was defined as the vertical distance between the collision site at the end of the rotary tillage blade and the plane in which the FUM was placed.

2.3.2 Determination of the level of collision test factors

The test bench and FUM structure determined the test factors: the width of the rotary tillage blade cutter edge, the rotational speed of the rotary tillage blade (equivalent collision height), and the collision direction of the FUM. Preliminary experiments indicated that the collision heights of the damage to the fixed and free FUM states are not identical. Specifically, the test results obtained for the fixed FUM have no reference value if the same test parameters used for the free FUM are used; therefore, it was necessary to consider the two sets of experiments separately.

(1) Determination of test level of rotary tillage blade cutter edge width

During the harvesting process, the collision damage to the FUM caused by the rotary tillage blade is random. Therefore, in this study, the collision energy loss between the rotary tillage blade and FUM particles was obtained using discrete element numerical simulations. The influence of rotary tillage blades of different widths on the FUM damage was indirectly evaluated based on the relationship between energy loss and damage[23].

As shown in Figure 6, Unigraphics NX 12.0 was used to build the geometric models of the soil-loosening mechanism and the rotary tillage blade with different cutter edge widths. These models were imported into Altair EDEM 2022 (EDEM). According to the better working speed interval of the existing whole machine loose soil hook and the rotational speed of the rotary tillage blade of the rotary tiller, the forward speed of the model was set to 0.6 m/s, and the rotation speed of the rotary tillage blade was set to 120, 160, 200, 240, and 280 r/min. Based on the minimum size of the largest FUM in the test materials, the maximum width of the blade was set to 10 mm. According to the equal division method, blade widths of rotary tillage blades were 2, 4, 6, 8, and 10 mm. The FUM and soil parameters[24,25] are listed in Table 1, and the two-factor five-level

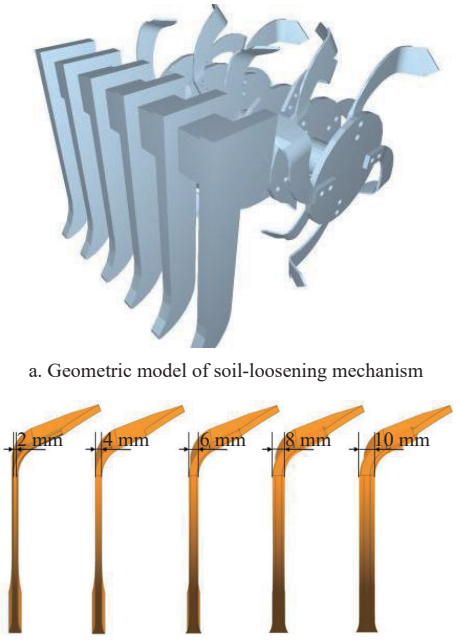

a. Geometric model of soil-loosening mechanism

b. Rotary tillage blades with five different cutter edge widths

Figure 6 Models used for the numerical simulation

random block test results are listed in Table 2. The contact models between soil particles were Hertz-Mindlin (no slip) and Hertz-Mindlin with bonding, and the motion models were rectilinear motion and rotational motion.

Table 1 Material parameters used in the discrete element numerical simulation

Material name		Material attribute name	Value
Soil	Soil - Soil	Poisson's ratio	0.38
		Solids density/kg·m^{-3}	2090
		Shear modulus/Pa	1.05×10^{6}
		Normal stiffness per unit area/N·m^{-3}	2.7×10^{8}
		Shear stiffness per unit area/N·m^{-3}	1.2×10^{8}
		Critical normal stress/kPa	180
		Critical shear stress/kPa	74
		Coefficient of restitution	0.2
		Coefficient of static friction	0.4
		Coefficient of rolling friction	0.22
	Soil - FUM	Coefficient of restitution	0.675
		Coefficient of static friction	1.04
		Coefficient of rolling friction	0.175
	Soil - Touch the soil components	Coefficient of restitution	0.25
		Coefficient of static friction	0.5
		Coefficient of rolling friction	0.015
FUM	FUM -FUM	Poisson's ratio	0.35
		Solids density/kg·m^{-3}	1104
		Shear modulus/Pa	1.3×10^{7}
		Coefficient of restitution	0.13
		Coefficient of static friction	0.3
		Coefficient of rolling friction	0.01
	FUM- Touch the soil components	Coefficient of restitution	0.38
		Coefficient of static friction	0.47
		Coefficient of rolling friction	0.097
Touch the soil components		Poisson's ratio	0.3
		Solids density/kg·m^{-3}	7865
		Shear modulus/Pa	7.9×10^{10}
Size of test groove		Length X/mm	1500
		Width Y/mm	500
		Height Z/mm	80

Table 2 Numerical simulation scheme and statistical results

No.	Width of cutter edge	Rotation speed/ r·min^{-1}	Energy loss/MJ	No.	Width of cutter edge	Rotation speed/ r·min^{-1}	Energy loss/MJ
1	2 mm	120	2.58	14	6 mm	240	8.77
2		160	4.28	15		280	11.17
3		200	5.84	16	8 mm	120	1.68
4		240	8.01	17		160	2.94
5		280	11.68	18		200	4.56
6	4 mm	120	3.36	19		240	4.83
7		160	4.81	20		280	4.94
8		200	5.98	21	10 mm	120	2.71
9		240	11.13	22		160	4.81
10		280	11.78	23		200	5.37
11	6 mm	120	2.30	24		240	6.73
12		160	4.76	25		280	8.36
13		200	5.11				

The numerical simulation results are presented in Figure 7. At a given cutter edge width, the energy loss increased monotonically as the rotational speed increased. For a given rotational speed, the

energy loss first increased, then decreased, and then increased again as the cutter edge width increased. A cutter edge width of 8 mm resulted in the smallest energy loss.

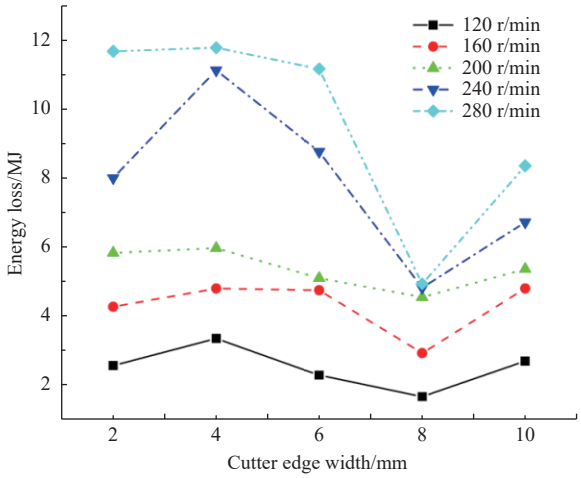

Figure 7 Energy loss as a function of cutter edge width for different rotational speeds

In practical production, FUM is in both the free and fixed states, and fixed FUM has more root tension than free FUM. Although the force of the blade and the FUM collision differed, the trends were the same. Therefore, this simulation only considered the collision between the blade and the FUM in the free state.

Based on the simulation results, the blade structure was modified, as shown in Figure 8 (Only the parts where impacts occur will be modified). Through stacking welding, the solder was piled up in the collision area of the blade, and the blade surface was polished.

a. Blade with 2-mm wide cutter edge (before modification) b. Blade with 8-mm wide cutter edge (after modification)

Figure 8 Two kinds of rotary tillage blades used in the test

(2) Determination of rotational speed of rotary tillage blade

Because the rotational speed of the blade cannot be simulated in a crash test, it was converted into the equivalent collision height according to

$$\begin{cases} v = \omega r = \sqrt{2gh} \\ \omega = \dfrac{2\pi n}{60} \end{cases} \tag{1}$$

where, r is the distance from the end of the rotary tillage blade to the center of the rotary tillage blade axis (18.3 cm), v is the speed at contact, ω is the angular velocity, n is the rotational speed, and h is the equivalent collision height.

The results of the calculations are listed in Table 3.

Table 3 Conversion between rotational speed and equivalent collision height

Equivalent collision height/mm	50	100	150	200	250	500	800	1100	1400
Rotational speed/r·min^{-1}	51.66	73.05	89.47	103.31	115.51	163.36	206.63	242.30	273.35

According to the preliminary test, the rotation velocities of the free and fixed FUM were different from those of the blade collision damage. For the free state, the equivalent collision heights were 200, 500, 800, 1100, and 1400 mm. For the fixed state, the equivalent collision heights were 50, 100, 150, 200, and 250 mm.

(3) Determining the collision direction

In actual harvesting, the collision direction between the blade and FUM is random; therefore, the three directions of the FUM were set as the test levels of the collision direction (see Figure 4).

2.3.3 Determination of the test scheme

Based on the abovementioned test factors and levels, an FUM collision damage test scheme was developed using a random block test, as listed in Table 4; among them, Nos. 1-30 are free FUM, and Nos. 31-60 are fixed FUM.

Table 4 Collision damage test scheme for free FUM

No.	Width of cutter edge	Collision direction	Equivalent collision height/mm	No.	Width of cutter edge	Collision direction	Equivalent collision height/mm
1			200	31			200
2			500	32			500
3		*X*	800	33		*X*	800
4			1100	34			1100
5			1400	35			1400
6			200	36			200
7			500	37			500
8	2 mm	*Y*	800	38	2 mm	*Y*	800
9			1100	39			1100
10			1400	40			1400
11			200	41			200
12			500	42			500
13		*Z*	800	43		*Z*	800
14			1100	44			1100
15			1400	45			1400
16			200	46			200
17			500	47			500
18		*X*	800	48		*X*	800
19			1100	49			1100
20			1400	50			1400
21			200	51			200
22			500	52			500
23	8 mm	*Y*	800	53	8 mm	*Y*	800
24			1100	54			1100
25			1400	55			1400
26			200	56			200
27			500	57			500
28		*Z*	800	58		*Z*	800
29			1100	59			1100
30			1400	60			1400

2.3.4 Determination of collision test index

FUM bulbs are irregular in shape, hollow inside, and of different sizes; therefore, the mass loss ratio was used to measure the damage to the FUM. The mass loss ratio was defined as the ratio of the damaged FUM mass to its original mass. The ink coloring method was used to determine the FUM damage. After each collision, the FUM was soaked in a 0.2% red ink-alcohol solution for more than 8 h[26,27], as shown in Figure 9.

After soaking, the excess FUM ink was wiped off and weighed on an electronic scale to observe the color of the FUM. The stained part of the collision site was cut off[28-30], and the remaining weight and mass loss ratio were recorded. The equation used to calculate

the mass loss ratio was

$$\eta = \frac{m_2}{m_1} \times 100\% \tag{2}$$

where, η is the mass loss ratio, m_1 is the FUM mass without damage, and m_2 is the FUM mass with the damage removed.

The results before and after the FUM was damaged are shown in Figure 10.

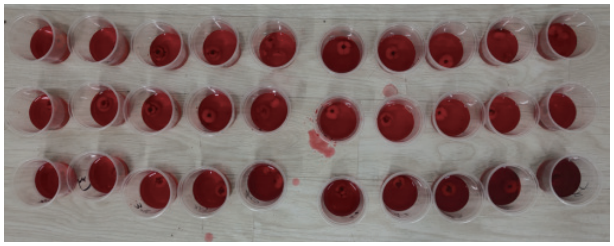

Figure 9 After each collision, the FUM was soaked in the dye to stain the damaged area.

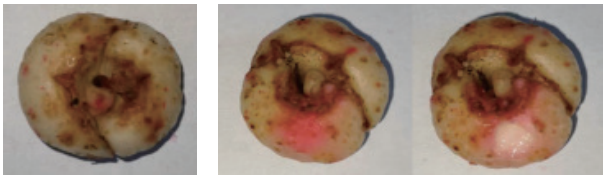

a. FUM with no damage b. Damaged FUM with stains (left) and damage removed (right)

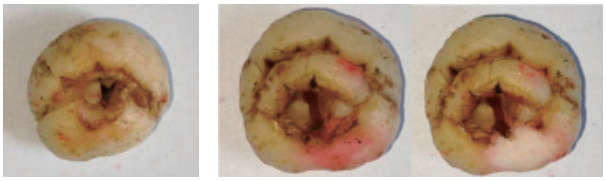

c. FUM with no damage d. Damaged FUM with stains (left) and damage removed (right)

Figure 10 Comparison of FUM damage

2.3.5 Relationship between energy loss and rotary tillage speed

The contact force of the cutting edge is shown in Figure 11.

In Figure 11, G is the weight of the FUM, F_f is the friction force exerted by the FUM, F_N is the supporting force exerted by the FUM, F_T and F'_T are the forces exerted by the rotary tillage blade on the FUM, and F'_{Tx} and F'_{Ty} are the forces exerted by the rotary tillage blade on FUM in the x- and y-directions. As shown in Figure 11, the cutter edge's width (2 mm) was relatively small compared to the thickness of the rotary tillage blade, and the cutter edge was a smooth arc. Therefore, the collision between the rotary tillage blade and the FUM occurred at an angle, which can be expressed as

$$\begin{cases} F'_{\mathrm{Tx}} = F'_{\mathrm{T}} \times \sin\alpha \\ F'_{\mathrm{Ty}} = F'_{\mathrm{T}} \times \cos\alpha \end{cases} \tag{3}$$

where, α is half of the angle between the edges, which was taken to be 5° when the edge width was 2 mm and 90° when the edge width was 8 mm.

According to Equation (3), when α is a constant value, F'_{Tx}, F'_{Ty} and F'_{T} are directly proportional to each other, and all of them increase as F'_{T} increases. The value of F'_{T} increases as the equivalent collision height increases; therefore, F'_{Tx} and F'_{Ty} also increase as the equivalent collision height increases. The increase in F'_{Ty} can be regarded as a further increase in the shear force, which makes FUM more prone to deeper damage.

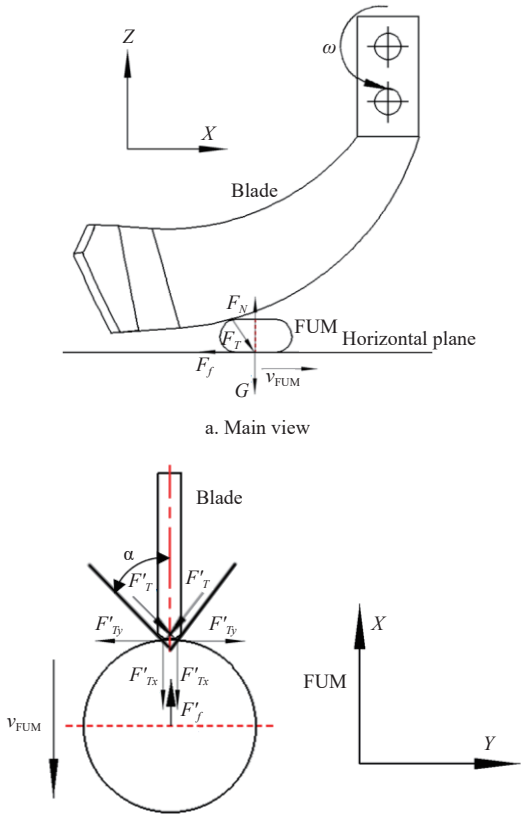

Figure 11 Diagram showing the collision force between the FUM and rotary tillage blade

2.3.6 The analysis of the collision process

The velocity of FUM before the collision is v_2, which is 0 because FUM is stationary before the collision, and the velocity of the rotary tillage blade is v_T. The velocity of FUM is v'_2 and the velocity of the rotary tillage blade is v'_T after the collision. According to the momentum conservation equation:

$$m_{\mathrm{R}} v_{\mathrm{T}} = m_{\mathrm{F}} v'_2 + m_{\mathrm{R}} v'_{\mathrm{T}} \tag{4}$$

where, m_R is the mass of rotary tillage blade, kg; m_F is the mass of FUM, kg; v_T is the velocity of the rotary tillage blade before impact, m/s; v'_T is the velocity of the rotary tillage blade after collision, m/s; v'_2 is the velocity of the rotary tillage blade after impact, m/s.

Definition of restitution coefficient e:

$$e = -\frac{v'_{\mathrm{T}} - v'_2}{v_{\mathrm{T}} - 0} \tag{5}$$

Then there is:

$$v'_{\mathrm{T}} - v'_2 = -e v_{\mathrm{T}} \tag{6}$$

Simultaneous Equations (4) and (6):

$$\begin{cases} m_{\mathrm{R}} v_{\mathrm{T}} = m_{\mathrm{F}} v'_2 + m_{\mathrm{R}} v'_{\mathrm{T}} \\ v'_{\mathrm{T}} = v'_2 - e v_{\mathrm{T}} \end{cases} \tag{7}$$

Substituting v'_{T} into the momentum conservation equation:

$$m_{\mathrm{R}} v_{\mathrm{T}} = m_{\mathrm{F}} v'_2 + m_{\mathrm{R}} (v'_2 - e v_{\mathrm{T}}) \tag{8}$$

Equation (8) is sorted out to obtain:

$$\begin{cases} v'_2 = \dfrac{m_{\mathrm{R}} \mathrm{v}_{\mathrm{T}} (1+e)}{m_{\mathrm{R}} + m_{\mathrm{F}}} \\ v'_{\mathrm{T}} = \dfrac{m_{\mathrm{R}} v_{\mathrm{T}} (1-e) - m_{\mathrm{F}} e v_{\mathrm{T}}}{m_{\mathrm{R}} + m_{\mathrm{F}}} \end{cases} \tag{9}$$

Total kinetic energy before impact:

$$E_B = \frac{1}{2} m_R v_T^2 \tag{10}$$

where, E_B is the impact kinetic energy of the rotary tillage blade, that is, the total kinetic energy before the impact, J.

Total kinetic energy after collision:

$$E_E = \frac{1}{2} m_F v_2'^2 + \frac{1}{2} m_R v_T'^2 \tag{11}$$

where, E_E is the total kinetic energy after the collision, J.

Then the loss energy caused by collision ΔE:

$$\Delta E = E_B - E_E \tag{12}$$

where, ΔE is the loss energy produced by the collision, J.

Substitute v_T' and v_2' into Equation (12):

$$\Delta E = (1 - e^2) \frac{m_F}{m_R + m_F} E_B \tag{13}$$

Since the mass ratio of FUM and rotary tillage knife is relatively fixed, let m_1=Km_2, then:

$$\Delta E = (1 - e^2) \frac{1}{K + 1} E_B \tag{14}$$

According to Equation (14), there is a linear relationship between the collision loss energy and the initial kinetic energy. As the collision energy increases, it will cause more energy losses, which are manifested in the form of FUM damage.

The kinetic energy theorem is introduced. According to Equations (3)-(14), the speed of the collision increases when the equivalent collision height increases, and the collision energy is proportional to the speed. The increase in collision energy results in a greater energy loss in the form of damage, which is similar to the results of other studies[31,32].

3 Results and analysis

3.1 Analysis of significance of FUM collision damage factors

The statistical results for the mean mass loss ratio of FUM are listed in Table 5. Among them, No. 1-30 are free FUM, and No. 31-60 are fixed FUM.

Table 5 Statistical results of average mass loss ratio for FUM

No.	Average mass loss ratio/%	No.	Average mass loss ratio/%	No.	Average mass loss ratio/%	No.	Average mass loss ratio/%	No.	Average mass loss ratio/%
1	0.00%	13	0.75%	25	2.24%	37	3.66%	49	5.28%
2	0.28%	14	1.12%	26	0.00%	38	3.03%	50	6.12%
3	1.44%	15	2.48%	27	0.00%	39	16.47%	51	0.26%
4	3.29%	16	0.00%	28	0.57%	40	19.01%	52	0.87%
5	3.55%	17	0.00%	29	0.87%	41	0.27%	53	1.79%
6	0.81%	18	0.28%	30	1.43%	42	0.55%	54	2.06%
7	1.00%	19	1.80%	31	1.06%	43	0.85%	55	4.00%
8	3.66%	20	2.43%	32	1.89%	44	1.45%	56	0.00%
9	3.87%	21	0.00%	33	3.05%	45	8.27%	57	0.26%
10	8.72%	22	0.87%	34	8.94%	46	0.50%	58	0.28%
11	0.00%	23	1.06%	35	21.67%	47	0.79%	59	0.75%
12	0.29%	24	1.34%	36	1.79%	48	1.41%	60	4.30%

3.1.1 Analysis of significance of FUM collision damage factors for free FUM

Statistical Product and Service Solutions (SPSS) software was used to analyze the results (Table 5 Nos. 1-30), as listed in Tables 6 and 7.

Table 6 Significance of mass loss ratio for free FUM according to an analysis of variance (ANOVA)

Source of variance	Degree of freedom	Sum of squares	Mean square	*F* value	Significance
Model	8	133.334	16.667	13.394	0.000
Width of cutter edge	1	11.241	11.241	9.034	0.007
Collision direction	2	13.319	6.660	5.352	0.013
Equivalent collision height	4	43.791	10.948	8.798	0.000
Error	22	27.375	1.244		
Total variation	30	160.708			

Table 7 Mean and standard error of mass loss ratios at different energy levels for free FUM

Main effect	Level	Number of observations	Mass loss ratio	
			Mean value	Standard error
Width of cutter edge	8 mm	15	0.860	0.845
	2 mm	15	2.084	2.307
Collision direction	*X*	10	1.308	1.403
	Y	10	2.357	2.564
	Z	10	0.750	0.785
Equivalent collision height	200 mm	6	0.136	0.332
	500 mm	6	0.407	0.430
	800 mm	6	1.293	1.226
	1100 mm	6	2.048	1.239
	1400 mm	6	3.476	2.656

Table 6 shows that the free FUM mass loss was extremely significant compared to that of the model. The width of the cutter edge, collision direction, and equivalent collision height significantly affected the FUM mass loss ratio, and the equivalent collision height was also extremely significant.

3.1.2 Analysis of significance of FUM collision damage factors for fixed FUM

SPSS was used to analyze these results (Table 5 Nos. 31-60), as shown in Tables 8 and 9.

Table 8 Significance of mass loss ratio for fixed FUM according to variance analysis (ANOVA)

Source of variance	Degree of freedom	Sum of squares	Mean square	*F* value	Significance
Model	8	1118.929	139.866	10.744	0.000
Width of cutter edge	1	133.545	133.545	10.258	0.004
Collision direction	2	81.201	40.6	3.119	0.064
Equivalent collision height	4	418.917	104.729	8.045	0.000
Error	22	286.4	13.018		
Total variation	30	1405.329			

Table 9 Mean and standard error of mass loss ratios at different energy levels for fixed FUM

Main effect	Level	Number of observations	Mass loss ratio	
			Mean value	Standard error
Width of cutter edge	8 mm	15	1.912	2.014
	2 mm	15	6.132	7.220
Collision direction	*X*	10	5.071	6.452
	Y	10	5.296	6.686
	Z	10	1.699	2.622
Equivalent collision height	50 mm	6	1.337	1.266
	100 mm	6	1.738	1.132
	150 mm	6	5.827	6.041
	200 mm	6	10.560	7.773
	250 mm	6	0.647	0.665

Table 8 shows that the fixed FUM mass loss was extremely significant compared to that of the model. The width of the cutter edge and the equivalent collision height had significant effects on the mass loss ratio of the FUM, whereas the collision direction was insignificant.

3.2 Single factor analysis of FUM collision damage

3.2.1 Influence of rotational speed on FUM damage

The mass loss ratio data listed in Table 5 were fitted using Origin 2021 (Origin). The fitted regression model and determination coefficient R^2 are listed in Table 10, and all the best-fit equations were significant.

Table 10 Regression of mass loss ratio for each grade and different factors (free FUM)

FUM status	Width of cutter edge	Collision direction	Regression model	Coefficient of determination R^2
Free FUM	8 mm	X	y= –0.875 22+0.002 22x	0.860
		Y	y= –0.218 57+0.001 65x	0.936
		Z	y= –0.422 04+0.001 24x	0.940
	2 mm	X	y= –0.981 47+0.003 37x	0.936
		Y	y= –1.369 34+0.006 23x	0.855
		Z	y= –0.616 46+0.001 93x	0.895
Fixed FUM	8 mm	X	y= –1.897 27+0.031 44x	0.870
		Y	y= –0.8044+0.017 35x	0.924
		Z	y=3.4533E-4·exp(x/26.606 62)+0.1378	0.997
	2 mm	X	y= –7.161 76+0.096 56x	0.789
		Y	y= –5.377 76+0.094 48x	0.821
		Z	y=(3.06107E-4)exp(x/24.6489)+0.488 02	0.998

3.2.1.1 Effect of rotational speed on the damage to free FUM

(1) Analysis of variation of FUM mass loss ratio in x-direction with equivalent collision height

As shown in Figure 12, the mass loss ratio in the x-direction was plotted against the equivalent collision height. At widths of 2 and 8 mm, the mass loss ratio increased as the equivalent collision height increased. The mass loss ratio caused by the 2 mm-wide blade was greater than that caused by the 8 mm-wide blade.

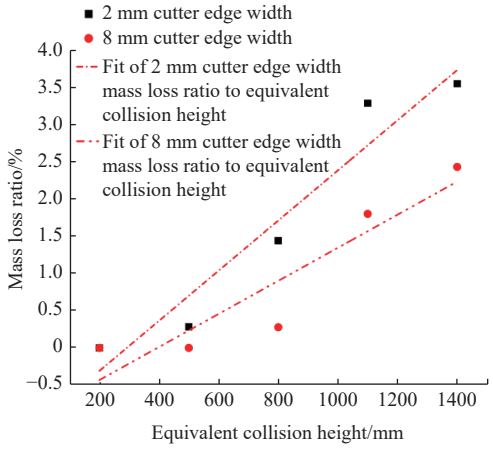

a. Best-fit lines for mass loss ratio and equivalent collision height in the x-direction

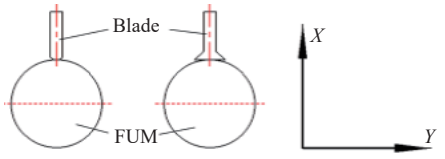

b. Diagram of collision direction in the x-direction

Figure 12 Mass loss ratio caused by the rotating tillage blade in the x-direction for free FUM

(2) Analysis of variation of FUM mass loss ratio in y-direction with equivalent collision height

As shown in Figure 13, the mass loss ratio in the y-direction was fitted to the equivalent collision height. At widths of 2 and 8 mm, the mass loss ratio increased as the equivalent collision height increased. The mass loss ratio caused by the 2 mm-wide blade was greater than that caused by the 8 mm-wide blade.

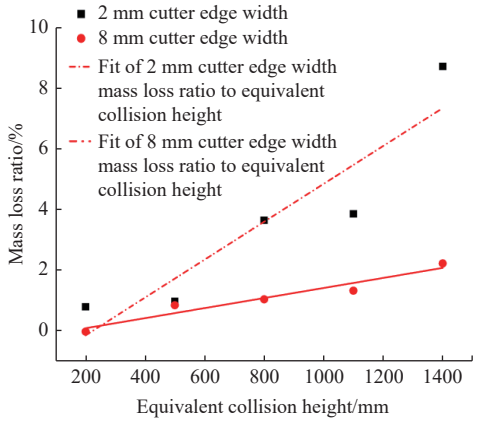

a. Best-fit lines for mass loss ratio and equivalent collision height in the y-direction

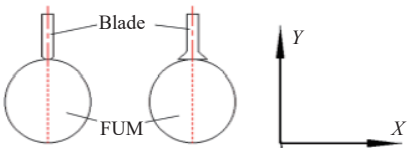

b. Diagram of collision direction in the y-direction

Figure 13 Mass loss ratio caused by the rotating tillage blade in the y-direction for free FUM

(3) Analysis of the variation of FUM mass loss ratio in z-direction with equivalent collision height

As shown in Figure 14, the mass loss ratio in the z-direction was fitted to the equivalent collision height. At widths of 2 and 8 mm, the mass loss ratio increased as the equivalent collision height increased. The mass loss ratio caused by the 2 mm-wide blade was greater than that caused by the 8 mm-wide blade.

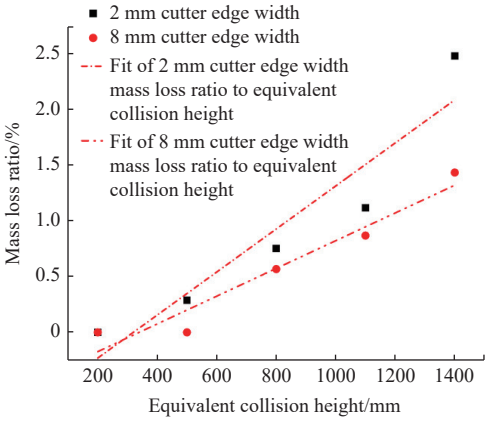

a. Best-fit lines for mass loss ratio and equivalent collision height in the z-direction

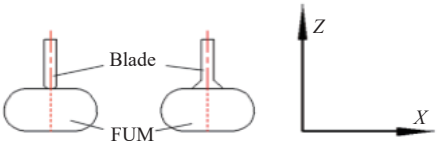

b. Diagram of collision direction in the z-direction

Figure 14 Mass loss ratio caused by the rotating tillage blade in the z-direction for free FUM

3.2.1.2 Effect of rotational speed on the damage to fixed FUM

(1) Analysis of variation of FUM mass loss ratio in *x*-direction with equivalent collision height

As shown in Figure 15, the mass loss ratio in the *x*-direction was fitted to the equivalent collision height. At widths of 2 and 8 mm, the mass loss ratio increased as the equivalent collision height increased. The mass loss ratio caused by the 2 mm-wide blade was greater than that caused by the 8 mm-wide blade.

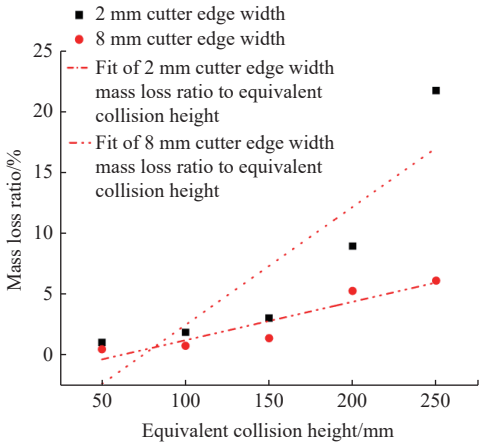

a. Best-fit lines for mass loss ratio and equivalent collision height in the *x*-direction

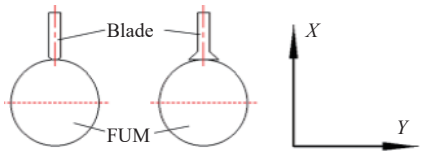

b. Diagram of collision direction in the *x*-direction

Figure 15 Mass loss ratio caused by the rotating tillage blade in the *x*-direction for fixed FUM

(2) Analysis of variation of FUM mass loss ratio in *y*-direction with equivalent collision height

As shown in Figure 16, the mass loss ratio in the *y*-direction was fitted to the equivalent collision height. At widths of 2 and 8 mm, the mass loss ratio increased as the equivalent collision height. The mass loss ratio caused by the 2 mm-wide blade was greater than that caused by the 8 mm-wide blade.

(3) Analysis of variation of FUM mass loss ratio in the *z*-direction with equivalent collision height

As shown in Figure 17, the mass loss ratio in the *z*-direction was fitted to the equivalent collision height. At widths of 2 and 8 mm, the mass loss ratio increased exponentially as the equivalent collision height increased. The mass loss ratio caused by the 2 mm-wide blade was greater than that caused by the 8 mm-wide blade.

For the equivalent collision height, owing to the test simulating the fixed FUM situation, the FUM was stuck to the test groove, restraining its movement. When the rotary tillage blade collided, the fixed FUM under the action of the decreasing collision motion caused more force to be exerted on the FUM. This also explains why the fixed FUM had a lower equivalent collision height than the free FUM.

3.2.2 Influence of collision direction on FUM damage

Table 8 shows that the collision direction caused no significant damage to the fixed FUM. Therefore, only the free FUM was analyzed. As shown in Table 8, the order of influence of the three directions on the mass loss ratio was *Y*>*X*>*Z*. The damage distribution was related to the FUM structure. According to a

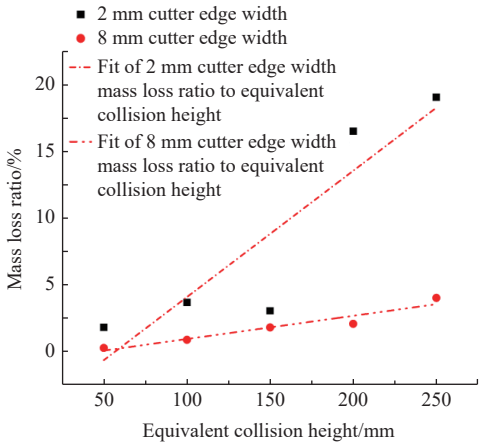

a. Best-fit lines for mass loss ratio and equivalent collision height in the *y*-direction

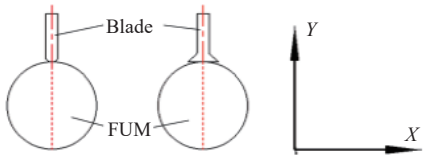

b. Diagram of collision direction in the *y*-direction

Figure 16 Mass loss ratio caused by the rotating tillage blade in the *y*-direction for fixed FUM

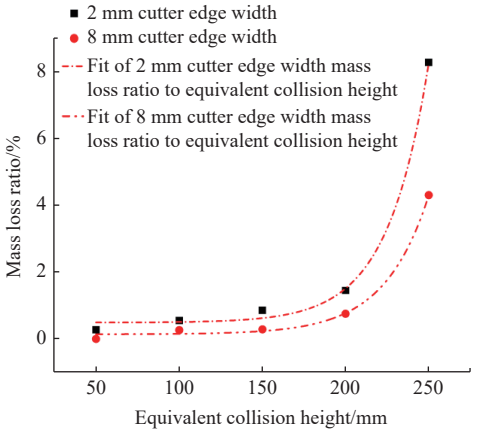

a. Best-fit lines for mass loss ratio and equivalent collision height in the *z*-direction

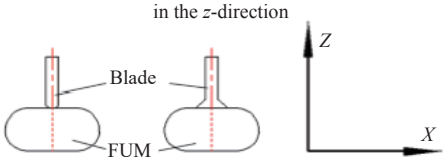

b. Diagram of collision direction in the *z*-direction

Figure 17 Mass loss ratio caused by the rotating tillage blade in the *z*-direction for fixed FUM

mechanical experimental study[33] and analysis of the FUM structure, the *y*-direction was the direction of the flap closure gap; thus, it was most vulnerable to damage. The *x*-direction of the FUM was formed by hugging at multiple scales. The side collision had no buffer and the force was large. The force required to cause damage to the rotary tillage blade and the absorption energy of the FUM were large. The *z*-direction was more compact than the *x*- and *y*-directions and was less susceptible to damage.

3.2.3 Influence of cutter edge width on FUM damage

Tables 9 and 10 indicate that the influence of the 2 mm-wide cutter edge on the FUM mass loss ratio was greater than that of the 8 mm-wide cutter edge.

According to the collision analysis, the reason for this can be observed in Equation (3). While α increases, F'_{Tx} increases and F'_{Ty} decreases. In addition, the larger the width, the smaller the force of the blade on the FUM in the y-direction and the greater the force on the x-direction, which is consistent with FUM mechanical tests[18]. The effect of the change in α on the force was consistent with the effect of the change in the angle on the force proposed by Kong et al.[34]

A shape analysis of the FUM revealed that it is an oblate sphere with small regional planes on its surface, as shown in Figure 18. Therefore, the collision between the FUM and the blade satisfied the pressure formula expressed as

$$P_T = \frac{F_T}{S} \tag{15}$$

where, P_T is the pressure exerted by the rotary tillage blade on the surface of the FUM, and S is the contact area between them.

Figure 18 FUM surface of a small area

According to Equation (15), P_T is only dependent on S, and the two are inversely proportional. Under the same force conditions, the wider the cutter edge, the lower the damage. Therefore, the damage to the FUM caused by the 8 mm-wide cutter edge was less than that caused by the 2 mm-wide cutter edge.

3.3 Relationship between energy loss and FUM damage

Comparing the free state FUM with the simulation data in EDEM, Figure 19 is obtained.

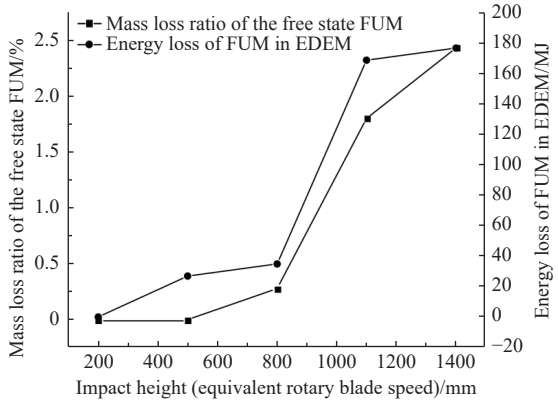

Figure 19 Statistical comparison of collision loss energy and mass loss ratio

It can be seen from Figure 19 that the change rule of collision loss energy and mass loss ratio are consistent with each other. The results shown in Figure 20 are obtained by fitting and correcting them.

Equation (16) was obtained through organization.

$$y = -0.306\,51 + 14.090\,37x \tag{16}$$

where, y is the mass loss ratio (damage) and x is the loss energy.

Therefore, the relationship between energy loss and FUM mass loss ratio (damage) can be determined by Equations (14) and (16). This conclusion illustrates that the higher the equivalent collision height, the greater collision damage of FUM.

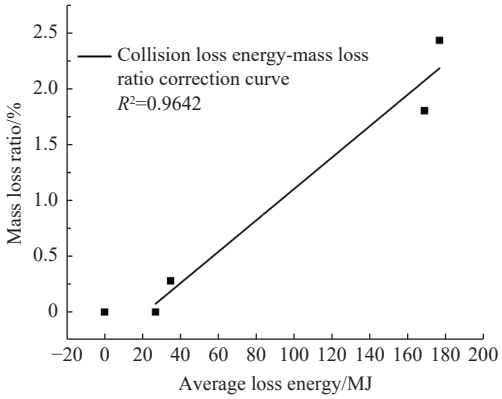

Figure 20 Collision loss energy-mass loss analogy curve after improvement

4 Discussion

There is a problem of bonded soil in fibrils of FUM. However, before rotary tillage, there will be a straight-handled loosening hook for loosening operations, which may result in a small amount of bonded soil in fibrils of FUM. The issue of bonded soil in fibrils of FUM will be solved more exactly in the future. Many various shapes of FUM exist naturally and most of the materials used in the experiment were selected manually, which resulted in a more unified shape being studied. The selection of the collision direction and position in the experiment was based on a specified position as the experimental parameter, which is challenging to determine during the actual loosening process. There are too many uncontrollable conditions in the field experiment which are impossible to accurately measure, such as soil viscosity, soil moisture content, and the size of FUM. Therefore, considering comprehensively, the method of building a test bed is used to carry out the preliminary test work. The actual application environment of the whole machine is complicated.

5 Conclusions

In this study, the *Fritillaria ussuriensis* Maxim (FUM) loosening mechanism was improved, and an FUM rotary tillage blade collision damage test bench was built. The effects of the rotational speed, cutter edge width, and collision direction on the mass loss ratio of the fixed and free FUM were analyzed. The results of the random block test showed that the influence factor model of the FUM mass loss ratio was significant. The rotational speed and cutter edge width had a significant influence on the mass loss ratio. The collision direction only had a significant influence on the free FUM, but not on fixed FUM. The single-factor test results showed that the mass loss ratio was linear and the coefficient of determination was greater than 0.789, and the mass loss ratio increased as the rotational speed increased. The order of the effect of the collision direction on the mass loss ratio of free FUM was $Y > X > Z$. The mass loss ratio of the 2 mm-wide cutter edge was greater than that of the 8 mm-wide cutter edge,and the minimum damage caused by the 8 mm-wide cutter edge was also determined. Energy loss and FUM damage were linear, and the coefficient of determination was 0.9642. By improving the rotary tillage blade,

the loss in harvest stage of FUM will be reduced and the yield of growers will be increased.

Acknowledgements

We acknowledge that this work was financially supported by University-targeted Training (Talent Introduction) Research Initiation Fund Project (Grant No. XDB202401), the Education Department of Heilongjiang Province for Heilongjiang Province "double first-class" discipline collaborative innovation achievement project (Grant No. LJGXCG2023-050), and the Ministry of Science and Technology of the People's Republic of China for integration and demonstration application of "up and down row" technology for eliminating obstacles and improving quality of soda saline soil (Grant No. 2023YFD1500605-0X).

[References]

[1] Song J, Yi S J, Liu L H. Two stage *Fritillaria ussuriensis* Maxim harvester. CN Patent CN110537410B. 2023-05-09. 2023.

[2] Zhang X Y, Li L Y, Pu J Z, Zhang Y Z. Traditional identification of *Fritillaria cirrhosa* and its common and easily confused products in the market. Journal of Anhui University of Chinese Medicine, 2023; 42(6): 92–96. (in Chinese)

[3] An Y L, Wei W L, Guo D A. Application of analytical technologies in the discrimination and authentication of herbs from *Fritillaria*: A review. Critical Reviews in Analytical Chemistry, 2022; 1–22. https://doi.org/10.1080/10408347.2022.2132374.

[4] Wang R C, Wang X Y, Qiao Y F, Li Y L. Research progress on the analysis of active ingredients and elements in *Fritillaria ussuriensis* Bulbus. Chinese Journal of Analytical Chemistry, 2022; 51(5): 100192.

[5] Zhao J Q, Zhao W, Tian S, Zhang Q, Song J, Li Y Q. Simulation test of soil covered parts of Fritillaria ussuriensis Maxim based on EDEM. Journal of Agricultural Mechanization Research, 2023; 45(10): 24–31.

[6] Lee K, Park S, Park W, Lee C. Strip tillage characteristics of rotary tiller blades for use in a dryland direct rice seeder. Soil & Tillage Research, 2003; 71(1): 25–32.

[7] Guo J, Zhang Q Y, Muhammad S, Ji C Y, Zhao Z. Design and experiment of bionic mole's toe arrangement serrated blade for soil-rototilling and straw-shattering. Transactions of the CSAE, 2017; 33(6): 43–50. (in Chinese)

[8] Yang Y W, Tong J, Ma Y H, Jiang X H, Li J G. Design and experiment of biomimetic rotary tillage blade based on multiple claws characteristics of mole rats. Transactions of the CSAE, 2019; 35(19): 37–45. (in Chinese)

[9] Jia H L, Ji W F, Han W F, Tan H J, Liu Z C, Ma C L. Optimization experiment of structure parameters of rototilling and stubble breaking universal blade. Transactions of the CSAM, 2009; 40(7): 45–50. (in Chinese)

[10] Zhang J, Xia M, Chen W, Yuan D, Wu C Y, Zhu J P. Simulation analysis and experiments for blade-soil-straw interaction under deep ploughing based on the discrete element method. Agriculture, 2023; 13: 136.

[11] Zhao H B, Li H W, Ma S C, He J, Wang Q J, Lu C Y. The effect of various edge-curve types of plain-straight blades for strip tillage seeding on torque and soil disturbance using DEM. Soil and Tillage Research, 2020; 202: 104674.

[12] Matin M, Fielke J, Desbiolles J. Furrow parameters in rotary strip-tillage: Effect of blade geometry and rotary speed. Biosystems Engineering, 2014; 118: 7–15.

[13] Matin M, Fielke J, Desbiolles J. Torque and energy characteristics for strip-tillage cultivation when cutting furrows using three designs of rotary blade. Biosystems Engineering, 2015; 129: 329–340.

[14] Matin M., Desbiolles J, Fielke J. Strip-tillage using rotating straight blades: Effect of cutting edge geometry on furrow parameters. Soil & Tillage Research, 2016; 155: 271–279.

[15] Lan J, Tang Q, Wu J, Yu W Y, Zhang M, Jiang D. Design and test of seedbed preparation machine before transplanting of rapeseed combined transplanter. Agriculture, 2022; 12: 1427.

[16] Yang Y S, Hu Z C, Gu F W, Ding Q H. Simulation and experimental study of the tillage mechanism for the optimal design of wheat rotary strip–tiller blades. Agriculture, 2023; 13: 632.

[17] Li S P, Hu H H, Wu L G. Optimum design and simulation analysis of drum screen for *Fritillaria* harvester. Journal of Agricultural Mechanization Research, 2022; 44(11): 46–53.

[18] Li S P, Wu L G, Wei X L, Man D W, Miao Z K. Experimental study and finite element analysis on bulb collision damage of *Fritillaria ussuriensis* Maxim. Journal of Agricultural Mechanization Research, 2021; 43(10): 126–131.

[19] Song J, Tian S, Wang Y S, Han X, Wang M, Sun X R. Analysis of impact and absorbed energy of *Fritillaria ussuriensis* Maxim during drum screening and its effect on impact damage. Computers and Electronics in Agriculture, 2023; 215: 108368.

[20] Song J, Tian S, Zhang Q, Wang L, Yi S J, Sun J B. Design and experiment on high efficient separating device of screening and kneading combined type for *Fritillaria ussuriensis* Maxim. Journal of Chinese Agricultural Mechanization, 2023; 44(9): 96–103.

[21] Song J, Wang Y S, Tian S, Sun X R, Yi S J. Analysis of impact damage of *Fritillaria ussuriensis* Maxim using a free drop experimental study. International Journal of Food Properties, 2023; 26(1): 1374–1389.

[22] Song J, Wang Y S, Xia R J, Tian S, Wang S B, Bian J Y. Analysis of collision damage of *Fritillaria ussuriensis* Maxim during drum screening. Journal of Food Process Engineering, 2024; 47(1): e1453.

[23] Xie S S, Deng W G, Liu F. Impact velocity and bruising analysis of potato tubers under pendulum impact test. Brazilian Journal of Agricultural and Environmental Engineering, 2023; 27(7): 559–566.

[24] Tian S, Wang Y S, Zhao W, Zhang Q, Wang S B, Lang J M. Comparative study on the screening performance of a vibrating screen with and without a kneading device, based on the discrete element method. Powder Technology, 2024; 434: 119301.

[25] Zhao S H, Liu H J, Tan H W, Cao X Z, Zhang X M, Yang Y Q. Design and performance experiment of opener based on bionic sailfish head curve. Transactions of the CSAE, 2017; 33(5); 32–39. (in Chinese)

[26] Fu H, He L, Ma S C, Karkee M, Chen D, Zhang Q. 'Jazz' apple impact bruise responses to different cushioning materials. Transactions of the ASABE, 2017; 60(2): 327–336.

[27] Rady A, Soliman N. Evaluation of mechanical damage of Lady Rosetta potato tubers using different methods. Postharvest Technology and Innovation, 2016; 5(2): 125–148.

[28] Zbigniew S, Krzysztof G. Studies concerning the response of potatoes to impact. International Agrophysics, 2022; 36: 115–122.

[29] Hussein Z, Fawole O, Opara U. Bruise damage susceptibility of pomegranates (*Punica granatum* L.) and impact on fruit physiological response during short term storage. Scientia Horticulturae, 2019; 246: 664–674.

[30] Fadiji T, Coetzee C, Chen L, Chukwu O, Opara U. Susceptibility of apples to bruising inside ventilated corrugated paperboard packages during simulated transport damage. Postharvest Biology and Technology, 2016; 118: 111–119.

[31] Celik H K, Ustun H, Erkan M, Rennie A, Akinci I. Effects of bruising of 'Pink Lady' apple under impact loading in drop test on firmness, colour and gas exchange of fruit during long term storage. Postharvest Biology and Technology, 2021; 179: 111561.

[32] Wang W Z, Zhang S M, Fu H, Lu H Z, Yang Z. Evaluation of litchi impact damage degree and damage susceptibility. Computers and Electronics in Agriculture, 2020; 173: 105409.

[33] Wang L, Zhao J Q, Song J, Wang Z L. Mechanics characteristics extrusion on *Fritillaria*. Journal of Northeast Agricultural Sciences, 2022; 47(5): 151–155.

[34] Kong X A, Jiang X Y, Jin X S. Solid contact mechanics. China Railway Publishing House, Beijing, 1999. (in Chinese)